CONF-950740--42

AN INTERIM REPORT ON SHALLOW-FLAW FRACTURE TECHNOLOGY DEVELOPMENT*

William E. Pennell, B. Richard Bass, John W. Bryson, and Wallace J. McAfee
Oak Ridge National Laboratory
Oak Ridge, Tennessee

ABSTRACT

Shallow-flaw fracture technology is being developed for application to the safety assessment of radiation-embrittled nuclear reactor pressure vessels (RPVs) containing flaws. Fracture mechanics tests on RPV steel, coupled with detailed elastic-plastic finite-element analyses of the crack-tip stress fields, have shown that (1) constraint relaxation at the crack tip of shallow surface flaws results in increased data scatter but no increase in the lower-bound fracture toughness, (2) the nil ductility temperature (NDT) performs better than the reference temperature for nil ductility transition (RT_{NDT}) as a normalizing parameter for shallow-flaw fracture toughness data, (3) biaxial loading can reduce the shallow-flaw fracture toughness, (4) stress-based dual-parameter fracture toughness correlations cannot predict the effect of biaxial loading on shallow-flaw fracture toughness because in-plane stresses at the crack tip are not influenced by biaxial loading, and (5) a strain-based dual-parameter fracture toughness correlation can predict the effect of biaxial loading on shallow-flaw fracture toughness.

INTRODUCTION

Pressurized-thermal-shock (PTS) loading produces biaxial pressure and thermal stress fields in an RPV wall. Thermal stresses are highest adjacent to the inner surface of the vessel where the effects of irradiation embrittlement and transient temperatures combine to produce the maximum reduction in the material fracture toughness. The net result of this combination of conditions is that the majority of predicted crack initiations originate from shallow flaws located on the inner surface of the vessel. The dominant influence of shallow surface flaws generates a need for an experimental investigation of (1) the effect of reduced crack-tip constraint on the material fracture toughness associated with shallow flaws, and (2) the effect of prototypical biaxial stress states on the material shallow-flaw fracture toughness, coupled with (3) development and validation of dual-parameter correlations that can be used to predict the material fracture toughness associated with shallow flaws in a biaxial stress field.

The U.S. Nuclear Regulatory Commission (NRC) is sponsoring shallow-flaw fracture technology research at Oak Ridge National Laboratory (ORNL) in the Heavy Section Steel Technology (HSST) Program. This paper presents an overview of recent developments in shallow-flaw fracture technology resulting from that research.

SHALLOW-FLAW FRACTURE TOUGHNESS

Fracture toughness tests have been performed on single-edge-notch-bending (SENB) test specimens using both deep (a/W = 0.5) and shallow (a/W = 0.1) flaws [1,2]. Beam specimens used in these tests are shown in Figs. 1 and 2. The beams tested by ORNL (Fig. 1) were fabricated from A 533 B material and were nominally 100 mm (4 in.) deep. Beams with a 230-mm-square (9-in.) cross section (Fig. 2) were cut from an RPV of a canceled nuclear plant and tested, under an HSST Program subcontract, by the National Institute for Standards and Technology (NIST). The inner-surface stainless steel cladding remained in place on the large-scale beams tested by NIST, and the flaws were located in the RPV longitudinal welds. Additional shallow-flaw fracture toughness data for A 533 B material were generated by the Fatigue and Fracture Branch of the Naval Surface Warfare

*Research Sponsored by the Office of Nuclear Regulatory Research, U.S. Nuclear Regulatory Commission under Interagency Agreement 1886-8011-9B with the U.S. Department of Energy under Contract DE-AC05-84OR21400 with Martin Marietta Energy Systems, Inc.

Center (NSWC) in Annapolis, Maryland [3]. Material for the NSWC tests was heat treated to increase its yield stress. The NSWC tests were also conducted using large (B = 89 mm, W = 83 mm) SENB specimens. Large-scale beams permitted testing of shallow flaws with depths in the range identified as critical for PTS analysis. Use of prototypical flaw depths reduced the uncertainties associated with extrapolation of shallow-flaw fracture toughness data for application to full-scale structures.

All data from Refs. 1-3 were generated using large-scale SENB specimens fabricated from RPV steel. They can, therefore, be combined into deep- and shallow-flaw data sets. In Ref. 4, these data sets were normalized in terms of both the reference temperature for nil-ductility transition (RT_{NDT}) and the nil ductility temperature (NDT). For the deep-flaw data, RT_{NDT} was found to be a satisfactory normalizing parameter (see Fig. 3). In contrast, the shallow-flaw data appeared to belong to two separate families, with quite separate lower-bound curves. The apparent existence of two separate families of data for a single material called into question the adequacy of RT_{NDT} as a normalizing parameter for the shallow-flaw fracture toughness of A 533 B plate and weld material. This problem was resolved when NDT was used as the normalizing parameter for all data points. Figure 4 shows that shallow-flaw fracture-toughness data from Refs. 1-3 form a homogeneous population when plotted as a function of T - NDT. A single curve defines the lower bound to the shallow-flaw fracture toughness data sets (Fig. 4). A comparison of Figs. 3 and 4 shows that the lower-bound curves for the deep- and shallow-flaw data are similar, but the mean fracture toughness and scatter of data are significantly higher for shallow flaws than for deep flaws.

BIAXIAL LOADING EFFECTS ON SHALLOW-FLAW FRACTURE TOUGHNESS

A typical biaxial stress field produced by PTS transient loading is shown in Fig. 5, together with a constant-depth shallow surface flaw. One of the principal stresses is seen to be aligned parallel to the crack front. There is no counterpart of this far-field out-of-plane stress in the shallow-flaw fracture toughness tests previously described. The far-field out-of-plane stress has the potential to increase stress triaxiality (constraint) at the crack tip and thereby reduce some of the fracture toughness elevation associated with shallow flaws. The HSST biaxial test program was instituted to investigate this effect.

A cruciform test specimen was developed at ORNL to investigate the effects of biaxial loading on the shallow-flaw fracture toughness of pressure vessel steels. Conceptual features of the specimen are shown in Fig. 6. The specimen design is capable of reproducing a linear approximation of the nonlinear biaxial stress distribution shown in Fig. 5. The cruciform test specimen design, coupled with a statically determinate load reaction system, permits the specimen to be loaded in either uniaxial (4-point bending) or biaxial (8-point bending) configurations. Tests of nominally identical specimens can thus be performed with the level of stress biaxiality as the only test variable.

An initial series of biaxial tests has been completed using test specimens fabricated from a single heat of A 533 B material. The biaxial load ratio is defined as P_T/P_L, where P_T is the total load applied to the transverse beam arms, and P_L is the total load applied to the longitudinal arms. Tests were run with P_T/P_L ratios of 0.0, 0.6, and 1.0. Details of those tests have been extensively reported [5,6] and will not be repeated here. K_{Jc} data from the biaxial tests are shown in Fig. 7, plotted as a function of the biaxiality ratio P_T/P_L. The plot shows a decrease in the lower-bound shallow-flaw fracture toughness with increasing biaxiality ratios. As the biaxiality ratio approaches 1.0, the lower bound to the shallow-crack toughness approaches that derived from SENB uniaxial deep crack data [1] for A 533 B steel. The data also indicate a trend of decreasing data scatter at a stress ratio of 0.6 when compared with the data scatter observed in both the uniaxial ($P_T/P_L = 0$) SENB shallow-flaw tests (see Fig. 4) and the biaxial shallow-flaw tests at a P_T/P_L loading biaxiality ratio of 1.0. In summary, the limited biaxial toughness data base, depicted in Fig. 7, provides evidence of a significant biaxial loading effect on cleavage fracture toughness in the transition temperature region for RPV steels.

DEVELOPMENT OF A DUAL-PARAMETER FRACTURE TOUGHNESS CORRELATION

Constraint Issues

Fracture initiates when limiting stress or strain conditions are exceeded at the tip of a crack. Stress-induced fracture initiates in a brittle material when the opening-mode stress exceeds a critical value over a finite length [7]. Strain-induced fracture initiates when crack-tip strains exceed the stress-state-dependent ductility of the material [8-11]. Crack-tip stress fields can be divided into hydrostatic and shear components. Yielding of the material, and the crack-tip blunting deformation that post-yield plastic deformation can produce, is governed by the shear component of the stress field. Tensile hydrostatic stresses contribute directly to the opening-mode tensile stresses but do not influence yielding or crack-tip blunting. It follows, therefore, that fracture toughness under stress-limiting conditions will be directly influenced when the hydrostatic component of the crack-tip stress field increases. Ductility controlled fracture toughness will be similarly influenced by increases in the hydrostatic component of the crack-tip stress field because of reduced crack-tip blunting, which increases the crack-tip strain concentration. Crack-tip constraint is the term used to describe conditions that influence the hydrostatic component of the crack-tip stress field.

Current fracture prevention technology relies on the use of fracture correlation parameters (K or J) to characterize both the applied loading and the resistance of engineering materials to crack initiation. Shortcomings of these conventional one-parameter fracture correlation methods, which have been well-documented in numerous references (e.g., see Refs. 12-15), are being addressed through development of various dual-parameter fracture methodologies. Dual-parameter, fracture-toughness correlations have been proposed to provide a quantitative assessment of the effects of reduced crack-tip constraint on fracture toughness. The existing dual-parameter methodologies being investigated within the HSST Program include stress-based fracture characterizations {e. g., J-Q methodology of O'Dowd and Shih [16-18] combined with Ritchie-Knott-Rice (RKR) fracture criteria [7] and the Dodds-Anderson (D-A) constraint correction technique [19]} and stress-strain-based characterizations {e. g., plane strain fracture ductility techniques of Tetleman and McEvily [8], Clausing [9], Barsom [10], Merkle [11], and other researchers}.

Determinations are being made concerning the bounds of applicability of the existing constraint effects correlation methodologies (i.e., how effective are they in matching existing

data?). The emphasis in these studies is placed on applications to measured data generated from both uniaxially and biaxially loaded shallow-crack fracture specimens. A major objective is to determine the effectiveness of the various methodologies in correlating measured toughness data in the transition temperature region of RPV steels. Evaluations that utilized applications of the stress-based correlations (i.e., J-Q and an engineering model [12] derived from the Dodds-Anderson methodology) were described in Ref. 6. Additional evaluations are described herein based on applications of two models to the ORNL cruciform specimen (Fig. 6), namely, the original formulation [19] of the Dodds-Anderson scaling model and an ORNL/HSST strain-based model [20, 21], incorporating plastic zone width in the crack plane as a second parameter.

Stress-Based Methodologies

The stress-based dual-parameter fracture methodologies[12, 16-19] utilize the effects of crack-tip constraint on in-plane stresses at the crack tip to infer the effect of constraint on fracture toughness. In Ref. 6, both the J-Q methodology and the D-A constraint scaling model were applied to shallow- and deep-crack SENB specimens [1] and to uniaxially and biaxially loaded cruciform specimens. Analysis results from these applications indicated that both methodologies could be used successfully to interpret experimental data from the shallow- and deep-crack uniaxially loaded SENB specimen tests. Figures 8 and 9 summarize an application of the D-A constraint correction model to fracture-toughness data from the HSST shallow-crack SENB program. In Fig. 8, the shallow- and deep-crack toughness data are plotted as a function of crack depth for a normalized temperature range of –10°C to –25°C. As expected in a low-constraint geometry, Fig. 8 shows both an increase in the mean fracture-toughness value and in data scatter from the shallow-crack specimens when compared with data from the deep-crack specimens. The corresponding toughness data, following application of the D-A correction model, are shown in Fig. 9. Results from the regression analysis, shown in Fig. 9, imply that the corrected toughness data are essentially independent of crack depth.

Applications of the J-Q and D-A constraint methodologies to the uniaxially and biaxially loaded cruciform specimens in Ref. 6 gave results that were considerably more difficult to interpret than those of the SENB specimens. The uniaxially loaded cruciform specimen analyzed in Ref. 6 failed at a sufficiently high load that the far-field bending stress began to impinge on the near-tip stress fields, a factor that rendered the J-Q results inconclusive. A modified D-A scaling procedure employed in Ref. 6 resulted in a J_{FB}/J_0 ratio (J_{FB} = J finite body; J_0 = J infinite body) for biaxial 0.6 loading that was ~ 25% greater than that for uniaxial loading. This implies a greater constraint loss for biaxial 0.6 loading than for uniaxial loading, a result inconsistent with toughness determined from the experimental data. The results from the D-A approach, however, were obtained using an engineering model developed by Dodds et al. [12] that approximates the scaling factors (J_{FB}/J_0) of the original D-A model. In the original formulation [19], toughness data are adjusted to small-scale yielding (SSY) values based on ratios of areas (or volumes) within principal stress contours around the crack tip. The engineering model applied to the cruciform specimens approximates these ratios using the stress distribution in the crack plane directly ahead of the crack tip, using a J-Q description of the crack-tip fields. Thus, the engineering model assumes that the stressed areas are similarly shaped, allowing the comparison of distances ahead of the crack rather than areas (or volumes). In Ref. 6, the possibility was raised that the engineering model may not be suitable for the cruciform specimen that possesses 3-D stress fields that vary through the thickness of the test section.

Because of these uncertainties concerning applications of the D-A engineering model in Ref. 6, the cruciform bend specimen was re-analyzed using the original formulation of the D-A scaling model based on stressed areas and volumes. Maximum principal stress contours in the range $2.5\sigma_0$ to $2.8\sigma_0$ (σ_0 = yield stress) enclose critical areas (or volumes) ahead of the crack tip, where cleavage fractures initiate. For the present study, maximum principal stress contours defined by $\sigma_1/\sigma_0 = 2.5$ were obtained at several positions along the crack front for a number of load steps up to 190 kips longitudinal load, using the ABAQUS-POST [22] computer program. The contour areas were then determined and plotted against the ABAQUS computed J-values for the respective crack front location and load value. From these curves, J-values for uniaxial and biaxial loading that give the same stressed areas can be determined and plots of J_B vs J_U can then be constructed (J_B is J for the biaxially loaded specimen, and J_U is J for the uniaxially loaded specimen).

The following results were obtained from application of the D-A scaling procedure to the 0.6 biaxial loading case: (1) self-similar principal stress areas were obtained with increasing load for both uniaxial and biaxial loading; (2) both maximum principal stress areas and J were essentially constant for the center 1.5 in. of the specimen, and then both area and J decreased rapidly as the crack-slot juncture was approached; (3) on average, the fact that J_B was somewhat greater than J_U agrees with the "modified" procedure employed in Ref. 6 and implies greater constraint loss for 0.6 biaxial loading than for uniaxial loading. This result is contrary to the experiments to date. A comparison of the results for J_B (0.6 biaxial loading) vs J_U is shown in Fig. 10.

The D-A scaling procedure was also applied to the P_T/P_L = 1.0 biaxial loading test because of the significantly reduced toughness result obtained in one of the tests (BB-10). A comparison of the D-A scaling procedure for J_B vs J_U is shown in Fig. 11 for the $P_T/P_L = 1.0$ biaxial loading case. Because the D-A methodology predicts a small biaxial effect on constraint, the predicted failure J for biaxial loading is essentially equal to the measured value for uniaxial loading. However, the predicted J value is substantially higher than the measured J from the lower-bound toughness of the $P_T/P_L = 1.0$ biaxial loading experiments (see Fig. 7).

The implication of the foregoing results, and those described in Ref. 6, is that the D-A and J-Q methodologies that are applied to in-plane stress fields at the crack tip do not adequately describe the effect of biaxial loading on fracture toughness. In an attempt to better understand these results, additional FEAs were performed on the cruciform specimen to clarify the relationship between biaxial loading ratio and development of the stress fields and plastic zone in the near crack-tip region. The stress components referenced in this discussion are calculated at the nodal location (N-5006), identified in Fig. 12, at a distance r = 2.5 mm (0.1 in.) from the crack tip; the coordinate system is given in the same figure.

Analysis results indicate that the point located at r = 2.5 mm (0.1 in.) experiences yielding at different load levels, depending on the out-of-plane loading ratio. According to the von Mises

yield criterion, yielding occurs when the second deviatoric stress invariant, J_2, reaches a critical value,

$$\sqrt{J_2} = K , \tag{1}$$

where

$$J_2 = (1/6)[(P_1 - P_2)^2 + (P_2 - P_3)^2 + (P_3 - P_1)^2] \tag{2}$$

Here, P_1, P_2, and P_3 are the principal stresses. The above yield criterion can be written in terms of the effective stress, σ_{eff}, according to

$$\sigma_{eff} = \sqrt{(3 \cdot J_2)} = \sqrt{3} \cdot K . \tag{3}$$

The Mises effective stress and, consequently, the yield criterion are governed by the differences in the principal stresses.

Relevant stress components (Cartesian normal stresses, hydrostatic stress, and Mises effective stress) are plotted in Figs. 13-15 to provide a better understanding of plastic zone development in the cruciform specimen. In Figs. 13-15, the Cartesian normal stress components (σ_{11}, σ_{22}, σ_{33}) represent good approximations to the magnitude of the principal stress values (the shear stress components are small). Applications of increasing ratios for out-of-plane to in-plane loading are accompanied by substantial elevations of the hydrostatic stress and the out-of-plane normal stress (σ_{11}). In contrast, the in-plane normal stress components (σ_{22}, σ_{33}) do not change a great deal as a function of load ratio, except at the highest load levels.

Development of the plastic zone can be correlated with the applied biaxial loading ratio and resultant out-of-plane normal stress component (σ_{11}). For the $P_T/P_L = 0.0$ (uniaxial) loading case (Fig. 13), the out-of-plane component is well below the two in-plane components, and the onset of yielding occurs at a relatively low applied load. When the out-of-plane load is increased to $P_T/P_L = 0.6$ (Fig. 14), the out-of-plane component roughly tracks the lower in-plane component up to 578 kN (130 kips) and then begins to increase at a substantially higher rate. The effect of the $P_T/P_L = 0.6$ load ratio is to delay the onset of yielding to a much higher load [~756 kN (170 kips)] than was observed in the $P_T/P_L = 0.0$ load case.

For the $P_T/P_L = 1.0$ load case (Fig. 15), the out-of-plane component (σ_{11}) turns up and essentially tracks the opening-mode (maximum) stress component (σ_{33}) beyond the 667-kN (150-kip) load level. Also, the normal stress components (σ_{11}, σ_{33}) and the hydrostatic stress are observed to increase at a greater rate beyond 667 kN (150 kips). [In this load range, observe that the hydrostatic and the out-of-plane stresses for the 1.0 load case are substantially elevated above those of the 0.6 case (see Fig. 14).] Near the 667-kN (150-kip) level, the plastic zone width progresses abruptly through N-5006, and the node exhibits significant strain hardening. An increase in differences between principal stress components is reflected in the increasing Mises effective stress.

In summary, Figs. 13-15 illustrate that increasing the out-of-plane to in-plane biaxial loading ratio from 0.0 to 1.0 results in a substantial increase of the out-of-plane normal stress component, while the two in-plane components remain relatively unchanged (except at the highest loads). Thus, far-field biaxial stresses have little effect on in-plane stresses in the cruciform specimen. This effect is further illustrated in Fig. 16, which shows the variation of stress components at node 5006 as a function of the far-field biaxial stress ratio. As a consequence, conventional stress-based cleavage fracture methodologies formulated in terms of in-plane stress components cannot detect the biaxial toughness effect clearly demonstrated in the ORNL biaxial fracture toughness tests. This conclusion is supported by measured biaxial toughness data (Fig. 7) and results depicted in Figs. 10 and 11 from applications of the D-A scaling procedure to the biaxially loaded cruciform specimen.

Stress-Strain-Based Methodologies

Experimental and analytical investigations presented in the previous section show that out-of-plane biaxial loading has no significant effect on in-plane stresses ahead of the crack tip. However, biaxial loading does influence development of the crack-tip plastic zone in the direction of crack propagation. These results, as well as results from prior experimental/analytical studies (described below), suggest that a strain-based dual-parameter fracture-toughness correlation is appropriate for RPV steels in the transition temperature region. This section describes studies initiated within the HSST Program that attempt to characterize crack-tip conditions through development and application of strain-based dual-parameter fracture toughness correlation methodologies.

Fractographic data obtained from examinations of broken halves of uniaxially and biaxially loaded cruciform specimens [6] were found to be consistent with a strain-based fracture-toughness correlation. Figure 17(*a*) shows the normalized opening-mode near-crack-tip stress distributions obtained from finite-strain analyses of cruciform specimens; the stress distributions are plotted vs normalized distance in front of the crack tip. The finite-strain SSY solution is shown for reference. In Fig. 17(*b*), initiation toughness data are plotted vs normalized distance from the initial crack-tip locations to the cleavage initiation sites. These data incorporate crack initiation sites located in the region of the crack-tip process zone where strain is increasing, but stress is decreasing (i.e., to the left of stress peak A) with increasing applied load. The expectation is that a cleavage initiation event will be governed by a criterion that exhibits a rising near-tip field at the initiation site under increasing applied load.

Previous investigations of strain-based methodologies in the transition region include those of Tetleman and McEvily (T-M) [8], Clausing [9], Barsom [10], Merkle [11], Weiss [23], and Pennell [20-21]. Clausing [9] related the decrease in toughness associated with increased strength of structural steels to a decrease in plane-strain ductility. Barsom [10] and Merkle [11] developed expressions for K_{Ic} based on plane-strain ductility, both of which compared well with measured toughness data in the transition temperature region. Weiss [23] developed an analytical relation for fracture toughness based on the material fracture strain. The scoping analysis of Ref. 20 adapted the Weiss relation to provide an estimate of biaxial loading effects on cleavage fracture toughness for RPV steels. In Ref. 20, the ratio of toughness values (K_b/K_u) corresponding to equibiaxial and uniaxial loading conditions, respectively, is predicted to be 0.47. This predicted value compares with the lower-bound K_b/K_u ratio of 0.56 obtained from measured data for A 533 B steel. The agreement between analytical prediction and measured data provides further support for a strain-based dual-parameter fracture-toughness correlation for transition-range fracture toughness.

According to the T-M criterion [8] plastically induced fracture initiates in a ligament immediately adjacent to the blunted crack tip when the ligament strain reaches the fracture strain (ε_f) of the material. The T-M fracture criterion can be interpreted [8] as a limiting condition for absorption of energy by inelastic deformation of the crack-tip material. Using this interpretation, the effects of constraint on fracture toughness can be quantified by analyzing the response of the crack-tip material to increasing load and determining the radius of the blunted crack tip corresponding to the crack-tip ligament strain at fracture (ε_f). Direct application of the latter strain-based approach would require a finite-strain elastic-plastic finite element analysis to determine the crack-tip radius as a function of the ligament strain. To circumvent this computationally intensive approach, an alternative methodology has been proposed [21] that utilizes R, the plastic zone width in the plane of the crack, as a correlation parameter for fracture toughness. An important feature of this methodology is that the parameter R can be calculated accurately in a small strain analysis.

The case for using R as the second parameter in a strain-based dual-parameter fracture toughness correlation derives from the observation [8] that the crack-tip radius ρ is a function of the plastic zone width (R). The T-M analysis gives a linear relationship between ρ and R for the case of plane-stress boundary conditions and contained yielding. Analysis and test results from the biaxial test program were used to determine the appropriate form of an ρ:R relationship for use in the domain of plane-strain and generalized plane strain boundary conditions, with both contained and uncontained yielding.

Finite-strain elastic-plastic finite element analyses were performed to determine R and the center of rotation for each of the cruciform specimen tests. Estimates for the crack-tip-opening-displacement (CTOD) at fracture were derived using the proportional relationship of equation 4.

$$CTOD = \frac{CMOD \bullet (L_c - a)}{L_c} \qquad (4)$$

where L_c is the distance of the center of rotation from the tensile surface of the test specimen, a is the crack depth determined from examination of the test specimen fracture surface, and CMOD is the measured crack-mouth-opening displacement at fracture. The crack-tip radius was taken as (CTOD)/2. Results from this interpretation of the test data did not conform with a linear ρ:R relationship. A quadratic expression with ln(R) as the independent variable produced a good fit to the test data. The data and the fitted curve are shown in Fig. 18.

The minimum value of ρ obtained from analysis of the test data was 0.113 mm ($4.4 \bullet 10^{-3}$ in.). Cottrell [24] has studied the effect of notch radius on fracture toughness. His conclusion, based on data from very low temperature tests of notched-bar steel specimens, was that the trend of decreasing fracture toughness with decreasing crack-tip radius ceased when the crack-tip radius was less than 0.127 mm ($5.0 \bullet 10^{-3}$ in.). This minimum value of the effective notch radius is defined as ρ_0. The yield stress for the material used for the specimens studied by Cottrell was 1080 MPa (157 ksi). This compares with a yield stress of 440 MPa (64 ksi) for the HSST cruciform specimen material. In the absence of any other variable, one would anticipate that ρ_0 would increase as the material yield stress decreases. The admissibility of the lowest data point in Fig. 18 could be questioned because of the Cottrell result. Merkle [11], however, used a value of 0.05 mm ($2.0 \bullet 10^{-3}$ in.) for ρ_0 to generate notch-strain-based predictions of fracture toughness for A 533 B steel which matched measured fracture toughness values in the transition temperature region. The Merkle result indicates that ρ_0 considerations should not influence the curve of Fig. 18.

Development of an HSST strain-based dual-parameter methodology is focusing on correlations of the cruciform test results with simple functions of the plastic zone width R. The investigation of biaxial loading effects on ligament conditions, described in the previous section, provides the variation of R with applied load shown in Fig. 19; curves are given in Fig. 19 for each of the three biaxial load ratios that were investigated. The analyses revealed that increasing the P_T/P_L ratio from 0.0 to 0.6 effectively delays the onset of yielding to a much higher applied load. Further increase of the P_T/P_L ratio to 1.0 leads to a marked reduction in the plastic zone growth rate, followed by relatively abrupt uncontained yielding at an intermediate load level [at ~667 kN (150 kips)]. Subsequent behavior is essentially like that of the uniaxial case for load levels beyond those shown in Fig. 19. Thus, a material point ahead of the crack tip experiences yielding at different load levels, depending on the out-of-plane loading. Studies have been initiated within the HSST Program to further clarify cause-and-effect relationships among the R-parameter, the load level, and the biaxiality ratio that lead to the results for the cruciform specimen depicted in Fig. 19. It has been suggested [21] that the abrupt development of uncontained yielding in the $P_T/P_L = 1.0$ case may explain why some researchers, using small test specimens in which uncontained yielding was unavoidable, have reported no effects of biaxial loading on fracture toughness.

The ORNL/HSST strain-based constraint-effects model, incorporating R as a second parameter, was utilized to predict an effect of biaxial loading on fracture toughness. This approach is illustrated in Fig. 20 where the biaxial fracture-toughness data from Fig. 7 are plotted as a function of the natural logarithm of the plastic zone width [ln(R)]. The data conform essentially to a straight-line relationship when plotted as a function of ln(R). The ±22-MPa $\sqrt{m}$ uncertainty band in Fig. 20 represents the fracture-toughness locus for the A 533 B test material, corresponding to a single normalized temperature (T – NDT) of –10°C. A family of similar fracture-toughness loci would be required to span the full range of normalized temperatures that could be encountered in an RPV transient analysis.

In Fig. 21, K_J vs ln(R) loading trajectories for three P_T/P_L load ratios applied to the cruciform specimen are superposed on the fracture-toughness locus of Fig. 20. These trajectories have three distinct phases that are characterized by the growth rate for R. The range of fracture-toughness values possible at T – NDT = –10°C, for a given loading condition, is predicted by the intersection of the K_J vs ln(R) loading trajectory with this fracture-toughness locus. In Fig. 21, unique K_{Jc} values are predicted for the uniaxial ($P_T/P_L = 0.0$) and biaxial ($P_T/P_L = 0.6$) loading cases. The intersection of the K_J vs ln(R) trajectory for equibiaxial ($P_T/P_L = 1.0$) loading with the toughness locus predicts both low and high K_{Jc} values for this loading condition. In fact, these low and high toughness values were realized in tests of the biaxial ($P_T/P_L = 1.0$) loading case. These toughness data are shown in Fig. 7. Uncontained yielding that developed in two of the biaxial ($P_T/P_L = 1.0$) tests gave high toughness values that were similar to those of the uniaxial loading tests.

Implicit in the K_{jc}-ln(R) dual-parameter fracture toughness correlation is the assumption that fracture toughness in the transition temperature range is strain-controlled. Strain-controlled fracture initiates when strains in ligaments adjacent to the blunted crack-tip reach the stress-state-dependent fracture strain (ε_f) for the material. Energy absorbed in the crack-tip material in straining the point of fracture is the product of the plastic work expended per unit volume (W_p) and the volume of material involved in the fracture process. A plane- strain stress-state exists close to the tip of the blunted crack-tip, so ε_f remains constant for all blunted crack configurations. The fracture energy required to generate a unit area of new fracture surface (G_c) is therefore directly proportional to the length of the crack-tip ligament which is strained to ε_f. Cottrell [24] and Tetelman and McEvily [8] have proposed that the length of this ligament can be approximated as twice the radius of the blunted crack-tip. If the fracture toughness is strain controlled the fracture toughness should, therefore, vary as $\sqrt{\rho}$.

The ρ vs ln(R) curve of Fig. 18 and the mean K_{Jc} vs ln(R) locus of Fig. 20 were normalized to K_{Jc}/K_{JcR} and ρ/ρ_R curves where suffix R denotes the reference value of K_{Jc} or ρ at ln(R) = -3.89. The normalized K_{Jc}/K_{JcR} and ρ/ρ_R curves are shown in Fig. 22, together with the curve of $\sqrt{\rho/\rho_R}$. The curves of K_{Jc}/K_{JcR} and $\sqrt{\rho/\rho_R}$ are seen to be similar, substantiating the strain-controlled-fracture basis of the K_{Jc} - ln(R) dual-parameter fracture toughness correlation.

INTERIM CONCLUSIONS

- The lower-bound fracture toughness for A 533 B plate and weld metal is similar for both shallow- and deep-flaw data sets.
- Data scatter and mean values of fracture toughness are higher for shallow flaws than for deep flaws.
- NDT appears to be a better normalizing parameter than RT_{NDT} for shallow-flaw fracture toughness data.
- The ORNL biaxial specimen permits the effects of biaxial loading on shallow-flaw fracture toughness to be isolated and measured.
- Biaxial loading can produce reductions in the shallow-flaw fracture toughness that can be as high as 40% for equibiaxial loading.
- Stress-based dual-parameter fracture toughness correlations cannot predict the observed effects of biaxial loading on shallow-flaw fracture toughness.
- A strain-based dual-parameter fracture toughness correlation has been developed using K_{Jc} and ln(R) as the parameters.
- The K_{Jc}-ln(R) fracture toughness correlation performed acceptably when applied to the uniaxial and biaxial shallow-flaw fracture toughness data.

ACKNOWLEDGMENTS

The authors wish to acknowledge the support and encouragement provided by N. S. M. Malik (HSST Project Manager) and M. W. Mayfield (Chief, Materials Engineering Branch), of the USNRC.

REFERENCES

1. T. H. Theiss and D. K. M. Shum, Martin Marietta Energy Systems, Inc., Oak Ridge National Laboratory, "Experimental and Analytical Investigation of the Shallow-Flaw Effect in Reactor Pressure Vessels," USNRC Report NUREG/CR-5886 (ORNL/TM-12115), July 1992.
2. J. A. Keeney, B. R. Bass, W. J. McAfee, and S. K. Iskander, Martin Marietta Energy Systems, Inc., Oak Ridge National Laboratory, "Preliminary Assessment of the Fracture Behavior of Weld Material in Full-Thickness Clad Beams," USNRC Report NUREG/CR-6228 (ORNL/TM-12735), October 1994.
3. R. E. Link and J. A. Joyce, "Experimental Investigation of Fracture Toughness Scaling Models," *Constraint Effects in Fracture: Theory and Applications*, ASTM STP 1244, M. Kirk and A. Bakker, Eds., 1994.
4. B. R. Bass, J. A. Keeney, and W. J. McAfee, "Assessment of the Fracture Behavior of Weld Material From a Full-Thickness Clad RPV Shell Segment," PVP-Vol. xxx, ASME, 1995.
5. T. J. Theiss et al., Martin Marietta Energy Systems, Inc., Oak Ridge National Laboratory, "Initial Results of the Influence of Biaxial Loading on Fracture Toughness," USNRC Report NUREG/CR-6036 (ORNL/TM-12349), June 1993.
6. B. R. Bass, J. W. Bryson, T. J. Theiss, and M. C. Rao, Martin Marietta Energy Systems, Inc., Oak Ridge National Laboratory, "Biaxial Loading and Shallow Flaw Effects on Crack-Tip Constraint and Fracture Toughness," NUREG/CR-6132 (ORNL/TM-12498), January 1994.
7. R. O. Richie, J. F. Knott, and J. R. Rice, "On the Relationship Between Critical Tensile Stress and Fracture Toughness in Mild Steel," *J. Mech. Phys. Solids,* 21, 394-410 (1973).
8. A. S. Tetleman and A. J. McEvily Jr., *Fracture of Structural Materials*, John Wiley & Sons, Inc., New York, 1967.
9. D. P. Clausing, "Effect of Plastic-Strain State on Ductility and Toughness," *International Journal of Fracture Mechanics* 6 (1), 71 (March 1970).
10. J. M. Barsom, "Relationship Between Plane-Strain Ductility and K_{Ic} for Various Steels," *Journal of Engineering for Industry* (November 1971).

11. J. G. Merkle, Union Carbide Corp. Nucl. Div., Oak Ridge National Laboratory, "An Elastic-Plastic Thick-Walled Hollow Cylinder Analogy for Analyzing the Strains in the Plastic Zone Just Ahead of a Notch Tip," ORNL-TM-4071, January 1973.

12. R. H. Dodds, C. F. Shih, and T. L. Anderson, "Continuum and Micromechanics Treatment of Constraint in Fracture," University of Illinois, UILU/ENG-92-2014, November 1992.

13. R. M. McMeeking and D. M. Parks, "On Criteria for J-Dominance of Crack-Tip Fields in Large-Scale Yielding," pp. 175–194 in *Elastic-Plastic Fracture*, ASTM STP 668, American Society for Testing and Materials, 1979.

14. C. F. Shih and M. D. German, "Requirements for One Parameter Characterization of Crack Tip Fields by the HRR Singularity," *Int. J. Fract.* 17(1), 27–43 (1981).

15. A. M. Al-Ani and J. W. Hancock, "J-Dominance of Short Cracks in Tension and Bending," *J. Mech. Phys. Solids* (39), 23–43 (1991).

16. N. P. O'Dowd and C. F. Shih, "Family of Crack-Tip Fields Characterized by a Triaxiality Parameter: Part 1 – Structure of Fields," *J. Mech. Phys. Solids,* 39, 989–1015 (1991).

17. N. P. O'Dowd and C. F. Shih, "Family of Crack-Tip Fields Characterized by a Triaxiality Parameter: Part II–Fracture Applications," *J. Mech. Phys. Solids* 40, 939–963 (1992).

18. N. P. O'Dowd and C. F. Shih, "Two Parameter Fracture Mechanics: Theory and Applications," USNRC Report NUREG/CR-5958 (CDNSWC/SME-CR-16-92), Brown University, February 1993.

19. R. H. Dodds Jr., T. L. Anderson, and M. T. Kirk, "A Framework to Correlate a/W Ratio Effects on Elastic-Plastic Fracture Toughness (Jc)," *International Journal of Fracture,* 48, 1–22 (1991).

20. W. E. Pennell, "Heavy-Section Steel Technology Program: Recent Developments in Crack Initiation and Arrest Research," *Nucl. Eng. Des*. 255–266 (1993).

21. W. E. Pennell and W. R. Corwin, "Reactor Pressure Vessel Structural Integrity Research," *Proceedings of the U. S. Nuclear Regulatory Commission 22nd Water Reactor Safety Information Meeting*, NUREG/CP-0140.

22. ABAQUS Theory Manual, Version 5-3, (Hibbit, Karlson, and Sorensen, Inc., Providence, R. I., 1993).

23. V. Weiss, "Material Ductility and Fracture Toughness of Metals," *Proceedings of the International Conference on Mechanical Behavior of Materials, Kyoto, Japan, August 15–20, 1971*, The Society of Materials Science, Japan, 1972.

24. A. H. Cottrell, "Mechanics of Fracture in Large Structures," *Proceedings of the Royal Society of London*, Vol. 285, 10 (1965).

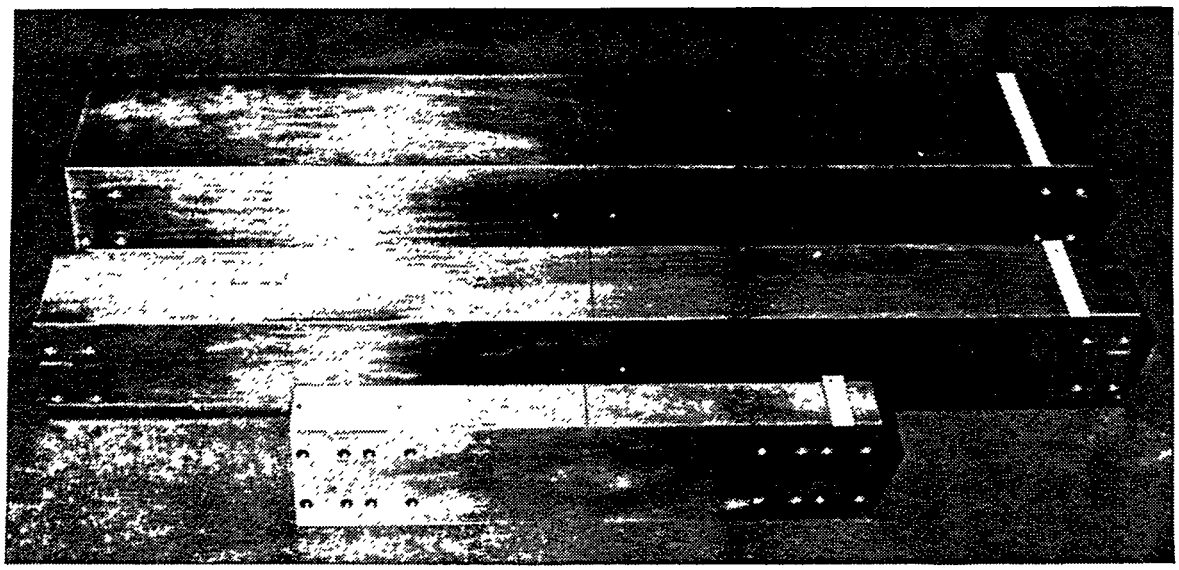

FIG. 1 THE 100-mm DEEP BEAMS WERE USED IN THE SHALLOW-FLAW TEST PROGRAM TO PERMIT FULL-SCALE TESTING OF SURFACE FLAWS HAVING DEPTHS IN THE RANGE THAT PTS ANALYSIS HAS SHOWN TO BE THE CONTROLLING RANGE FOR CRACK INITIATION.

FIG. 2 A LIMITED NUMBER OF FULL-SCALE BEAM SPECIMENS USED IN SHALLOW-FLAW TEST PROGRAM WERE CUT FROM THE SHELL OF AN RPV FROM A CANCELED NUCLEAR PLANT.

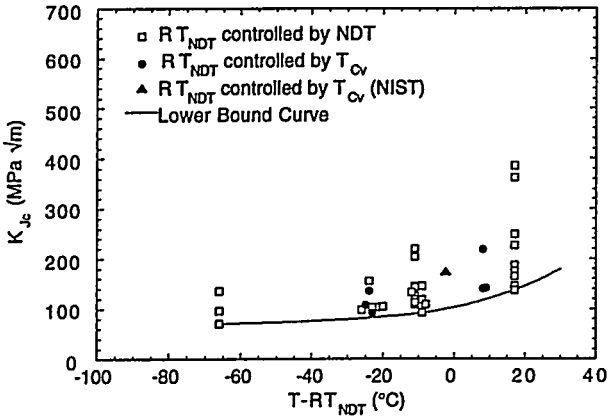

FIG. 3 THE PARAMETER-CONTROLLING RT_{NDT} HAS NO SIGNIFICANT EFFECT ON THE DISTRIBUTION OF K_{Jc} VS $T - RT_{NDT}$ DATA POINTS FROM THE DEEP-CRACK SENB A 533 B SPECIMENS. A SINGLE CURVE ADEQUATELY DEFINES THE LOWER BOUND FOR THE COMBINED DATA SET.

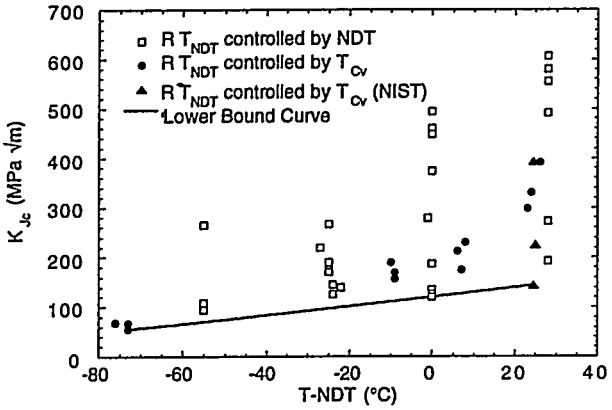

FIG. 4 SHALLOW-FLAW FRACTURE TOUGHNESS DATA FOR A 533 B PLATE AND WELD MATERIAL FORM A SINGLE HOMOGENEOUS GROUP WHEN PLOTTED AS A FUNCTION OF THE NORMALIZING PARAMETER T –NDT.

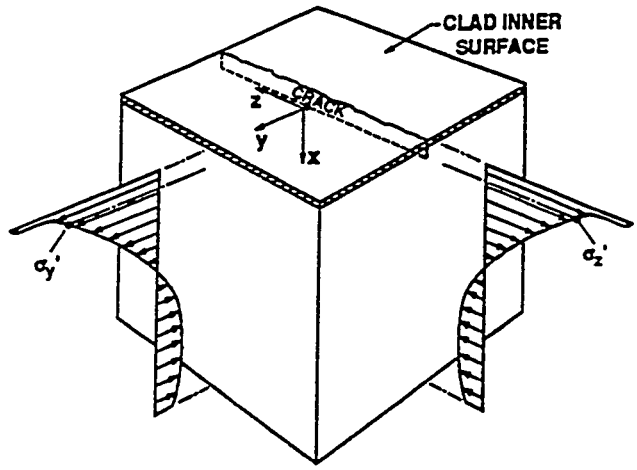

FIG. 5 PTS LOADING PRODUCES BIAXIAL STRESSES IN AN RPV WALL WITH ONE OF THE PRINCIPAL STRESSES ALIGNED PARALLEL WITH THE TIP OF A CONSTANT-DEPTH SHALLOW SURFACE FLAW.

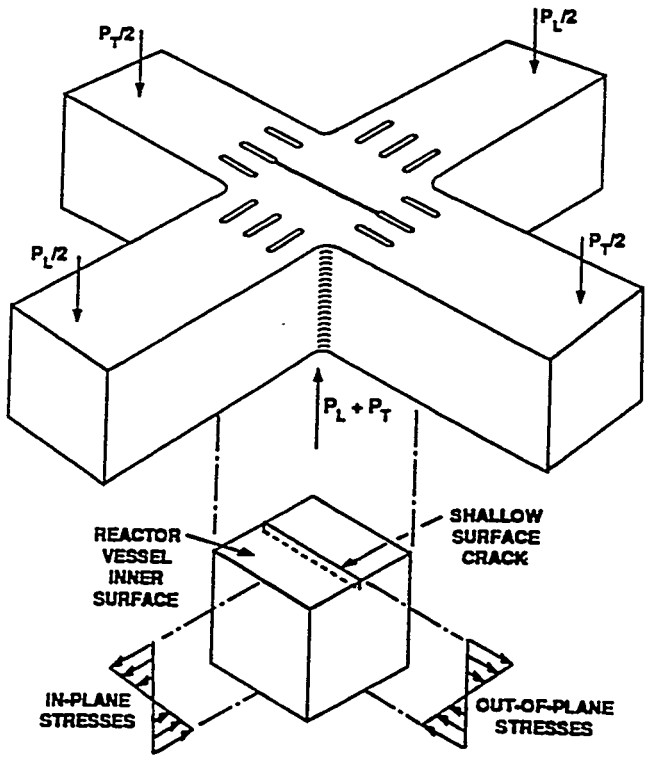

FIG. 6 CONCEPTUAL FEATURES OF THE CRUCIFORM SHALLOW-FLAW BIAXIAL FRACTURE TOUGHNESS TEST SPECIMEN.

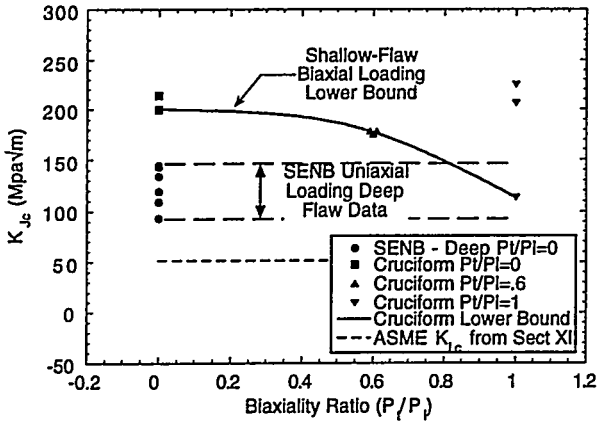

FIG. 7 DATA FROM A SINGLE HEAT OF A 533 B STEEL TESTED AT T–NDT = –10°C INDICATE THAT BIAXIAL LOADING REDUCES THE LOWER-BOUND TRANSITION-RANGE SHALLOW-FLAW FRACTURE TOUGHNESS.

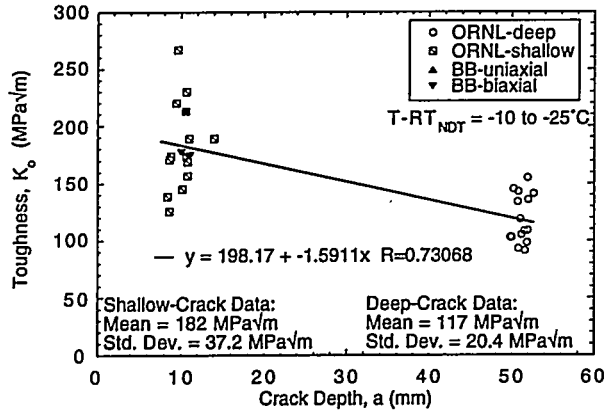

FIG. 8 MEAN VALUE AND SCATTER OF DATA FOR SHALLOW FLAWS ARE INCREASED WHEN COMPARED WITH DATA FOR DEEP FLAWS.

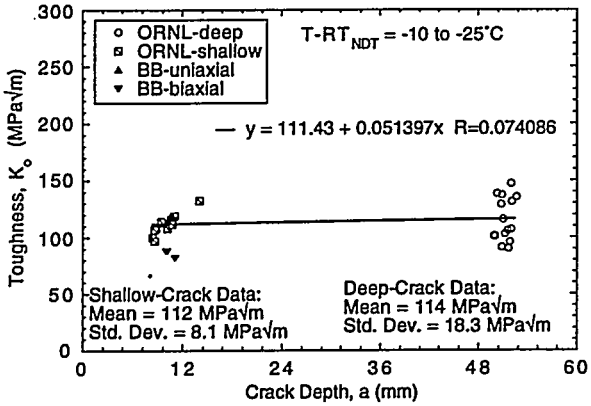

FIG. 9 APPLICATION OF THE D-A CONSTRAINT ADJUSTMENT PROCEDURE ELIMINATES THE CRACK DEPTH EFFECT ON FRACTURE TOUGHNESS.

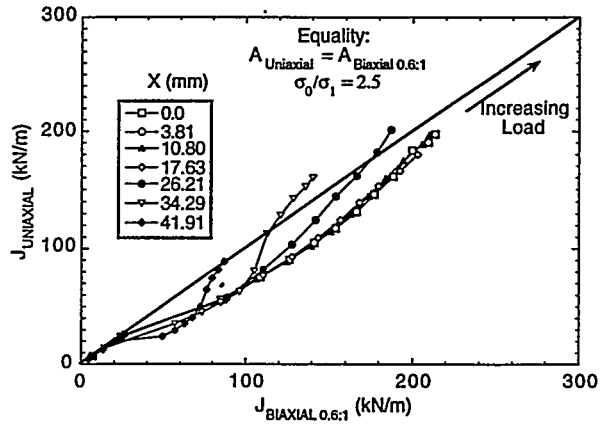

FIG. 10 VALIDATION CHECK ON THE D-A CONSTRAINT ADJUSTMENT FOR BIAXIAL (0.6:1) AND UNIAXIAL (0:1) TESTS.

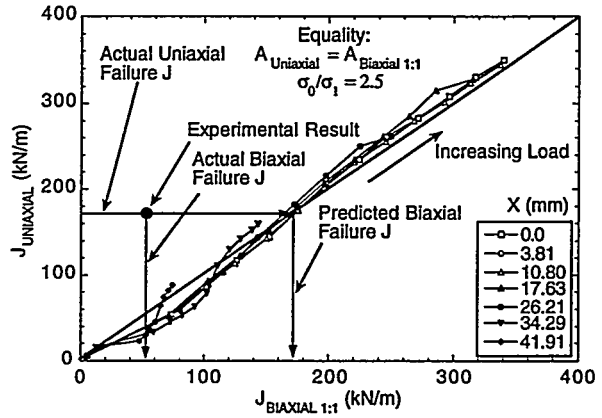

FIG. 11 VALIDATION CHECK ON THE D-A CONSTRAINT ADJUSTMENT FOR BIAXIAL (1:1) AND UNIAXIAL (0:1) TESTS.

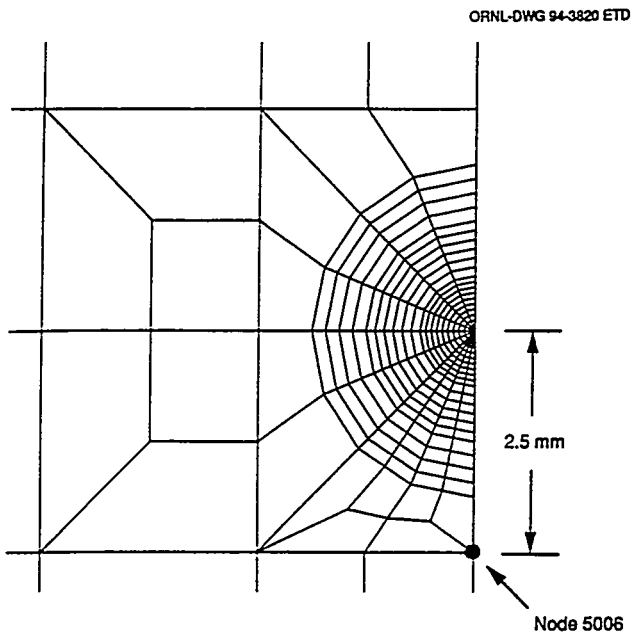

FIG. 12 THE EFFECT OF STRESS BIAXIALITY ON PRINCIPLE STRESSES WAS EXAMINED AT A POINT 2.5 mm (0.1 IN) AHEAD OF THE CRACK TIP.

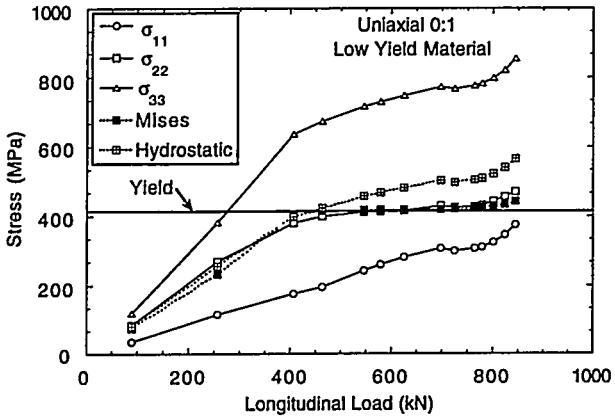

FIG. 13 STRESS COMPONENTS FOR UNIAXIAL LOADING AT A POINT 2.5 mm AHEAD OF THE CRACK TIP.

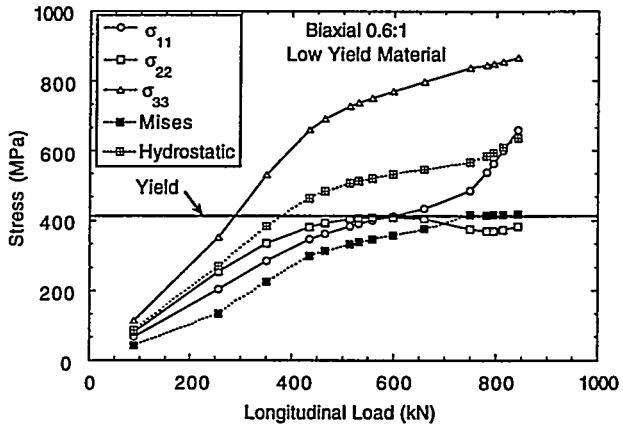

FIG. 14 STRESS COMPONENTS FOR 0.6:1 BIAXIAL LOADING AT A POINT 2.5 mm AHEAD OF THE CRACK TIP.

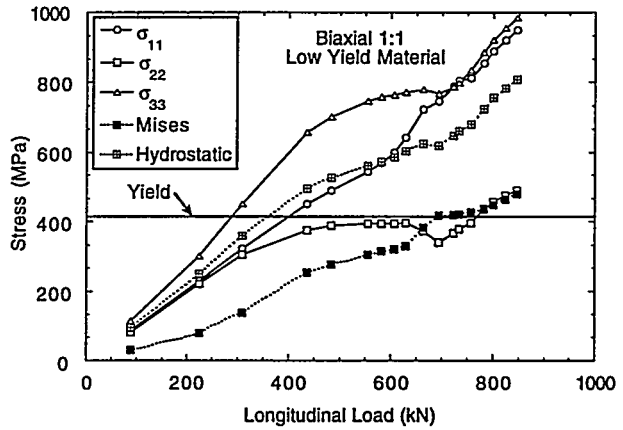

FIG. 15 STRESS COMPONENTS FOR 1:1 BIAXIAL LOADING AT A POINT 2.5 mm AHEAD OF THE CRACK TIP.

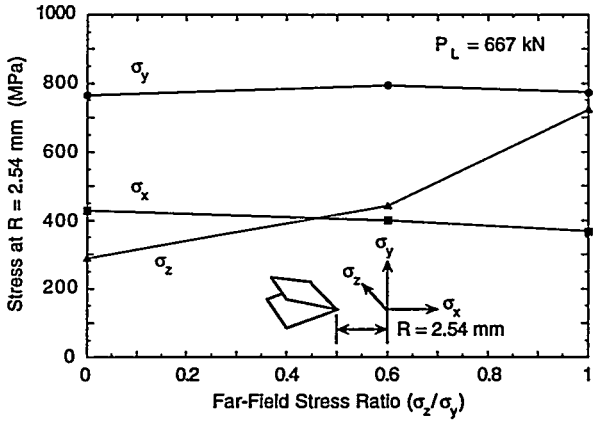

FIG. 16 FAR FIELD STRESS BIAXIALITY HAS LITTLE EFFECT ON IN-PLANE STRESSES NEAR THE CRACK TIP.

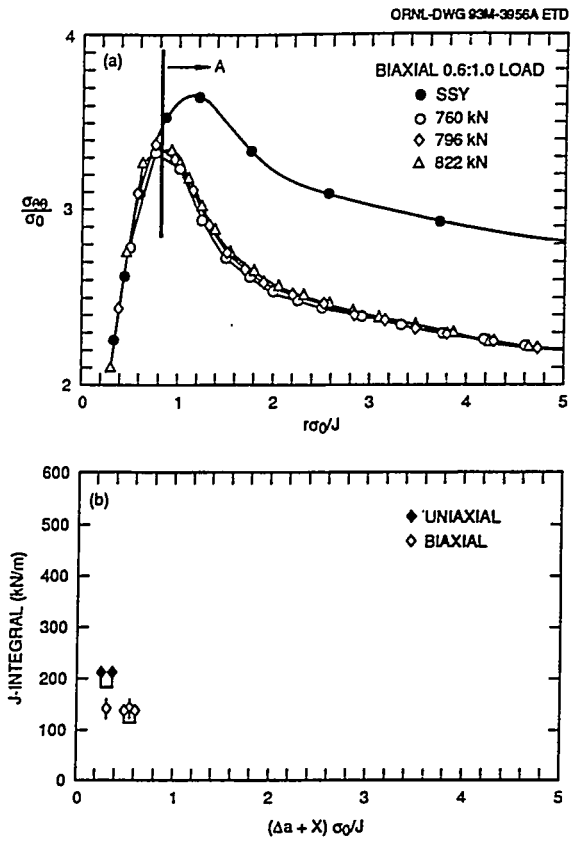

FIG. 17 FRACTURE INITIATION SITE LOCATIONS DETERMINED FROM FRACTOGRAPHIC DATA INDICATE THAT STRAIN BASED FAILURE MODES MAY GOVERN FRACTURE AT TEMPERATURES IN THE TRANSITION REGION.

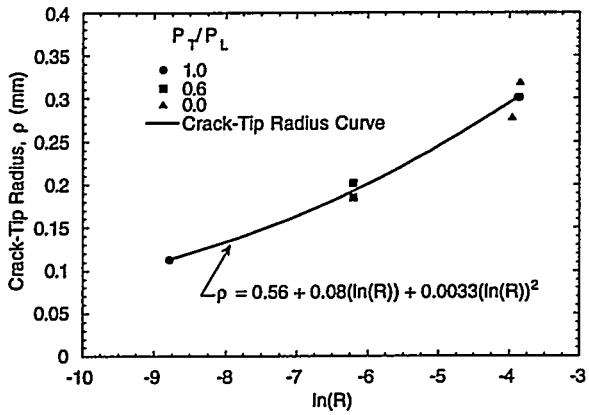

FIG. 18 A SECOND ORDER POLYNOMIAL CURVE WITH LN(R) AS THE INDEPENDENT VARIABLE FITS THE CRACK-TIP RADIUS DATA FROM BOTH UNIAXIAL AND BIAXIAL TESTS.

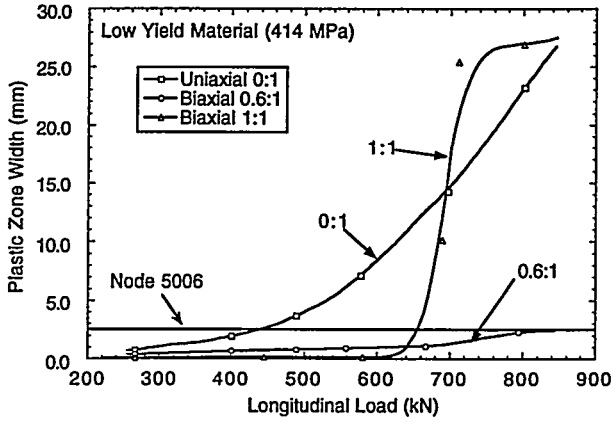

FIG. 19 THE RATE OF INCREASE OF THE WIDTH (R) OF THE CRACK-TIP PLASTIC ZONE IN THE DIRECTION OF CRACK PROPAGATION IS DIRECTLY RELATED TO THE BIAXIAL LOADING RATIO P_T/P_L.

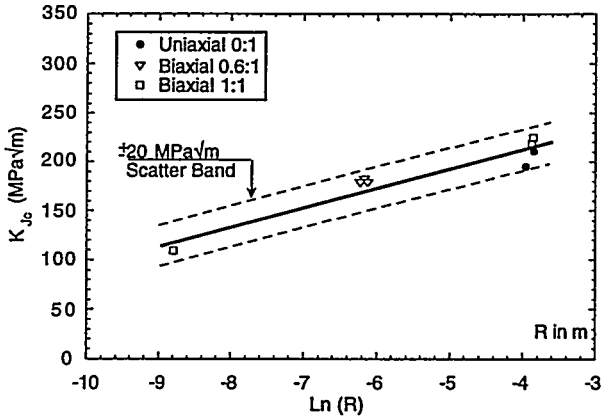

FIG. 20 TEST DATA AND ANALYSIS RESULTS FOR THE BIAXIAL SPECIMEN ARE COMBINED TO DEFINE A K_{Jc}-LN(R) SHALLOW-FLAW FRACTURE TOUGHNESS LOCUS.

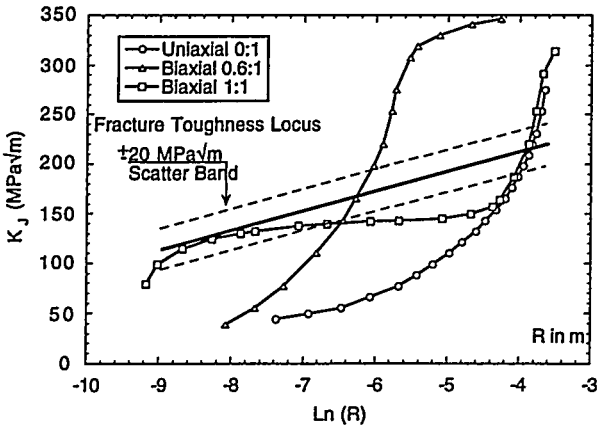

FIG. 21 K_{Jc}-LN(R) TRAJECTORIES FOR THE BIAXIAL SPECIMEN PREDICT UNIQUE K_{Jc} VALUES FOR UNIAXIAL AND P_T/P_L = 0.6 LOADING, BUT BOTH HIGH AND LOW K_{Jc} VALUES ARE POSSIBLE FOR THE P_T/P_L = 1.0 LOADING BECAUSE OF THE LOW YIELD STRESS OF THE MATERIAL USED FOR THESE TESTS.

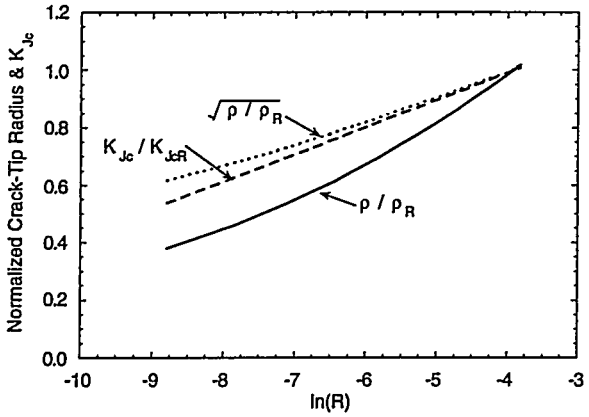

FIG. 22 THE CURVE REPRESENTING ρ/ρ_R IS SIMILAR TO THE CURVE OF K_{Jc}/K_{JcR}, INDICATING THAT FRACTURE IN THE TEMPERATURE RANGE COVERED BY THESE TESTS IS STRAIN CONTROLLED.